Journal of Materials Chemistry A

Tuning the performance of Mg negative electrode by grain boundaries and alloying toward the realization of Mg battery

Journal:	*Journal of Materials Chemistry A*
Manuscript ID	TA-ART-03-2021-002419.R1
Article Type:	Paper
Date Submitted by the Author:	30-Apr-2021
Complete List of Authors:	Tian, Hong Kang; National Institute for Materials Science, Jalem, Randy; Busshitsu Zairyo Kenkyu Kiko, ; Nagoya Institute of Technology, Materials Science and Engineering Matsui, Masaki; Kobe University, Department of Chemical Science and Engineering MANDAI, Toshihiko; National Institute for Materials Science, Center for Research on Energy and Environmental Materials Somekawa, Hidetoshi; Busshitsu Zairyo Kenkyu Kiko, Tateyama, Yoshitaka; National Institute for Materials Science, Center for Green Research on Energy and Environmental Materials (GREEN)

ARTICLE

Tuning the performance of Mg negative electrode by grain boundaries and alloying toward the realization of Mg battery

Received 00th January 20xx,
Accepted 00th January 20xx

DOI: 10.1039/x0xx00000x

Hong-Kang Tian,[a] Randy Jalem,[a,b,c] Masaki Matsui,[d] Toshihiko Mandai,[a] Hidetoshi Somekawa,[e] Yoshitaka Tateyama*[,a,b]

Persistent Magnesium (Mg) dissolution/deposition during cycling is crucial for the practical use of Mg rechargeable batteries, and the alloying-enhanced performance has recently attracted much attention. Nevertheless, the microscopic relationship among the alloys, the defects, and the performance remains under debate. Here, via comprehensive Density Functional Theory calculations, we revealed the effect of alloying-induced grain boundaries (GBs) and demonstrated a microscopic mechanism of how the GBs and alloys affect the performance. Mg atoms at [0001]($10\bar{1}0$) tilt GB and ($11\bar{2}0$) surface are preferentially stripped during discharge, resulting in a "pit-type" morphology. Surprisingly, alloying does not change the Mg's dissolution tendency at GB. Instead, it can tune the amount of tilt GBs, as alloying with Ca or Na can create more GBs than Li, Al, and Zn, resulting in improved discharge performance. Considering the experimental observation, we also propose a new picture of a GB-dependent electrochemical energy diagram extending from the conventional electrochemical theory.

Introduction

Mg is a desired negative electrode (NE) material for Mg rechargeable batteries (MRBs) because of its high theoretical capacity of ~2200 mA/g, low reduction potential (-2.37 V vs. standard hydrogen electrode), low cost due to the abundance in the Earth, and environmentally benign.[1,2] Pure Mg NE, however, suffered from the formation of the passivation layer at the surface that blocks Mg-ions to transfer.[3,4] Alloying with specific metal elements has been intensively studied as a primary method to mitigate the issue above, owing to making the reaction products detached and further suppress the parasitic corrosion.[5] Several alloying elements have been reported, such as Li, Al, Sn, Li, Zn, Pb, and Ca.[6–14] The dissolution/deposition performance of the pure Mg and Mg alloy NE appear to be highly affected by the microstructures, such as secondary phases,[15,16] grain orientation,[17–19] and grain boundaries (GBs).[20,21] Nevertheless, whether the grain boundaries improve the dissolution/deposition rate has been under argument, and the hidden mechanism is still unclear. To further improve the performance of MRBs, it is essential to clarify the role of GBs in the performance of Mg and Mg-alloy NE.

There are controversial discussions concerning the effect of GBs on the dissolution of Mg alloys. Aung et al.[22] and Jiang et al.[23] observed that Mg alloys' dissolution rate dropped with the grain size decrease. Because the smaller grain size results in a higher GB density, it is believed that the GBs serve as dissolution barriers based on their results. On the other hand, Shi et al.[24] and Zhang et al.[25] proposed that the existence of GBs reduces the dissolution resistance of Mg alloys. In their studies, decreasing the grain size led to a higher dissolution rate, implying that the Mg atoms at GB are easier to be stripped. Due to these conflicts, GB's role in the dissolution reaction has not been fully determined yet.

Computational studies on the atomic scale can provide information that helps to reveal the hidden mechanism. Several calculation studies have been done for the pure Mg and Mg alloys. For example, the GB segregation energy of different dopants was computed to evaluate the dopant's aggregation tendency at the twin grain boundaries (TB) in Mg alloys.[26–28] Ma et al.[29] proposed that the calculated surface energy and work function of surface models based on TB structure can be used to study the anodic dissolution of pure Mg and Mg alloys. However, these studies focused only on TBs, a relatively ideal and simplified case in terms of defects, which may be insufficient to mimic the real situation. Therefore, to elucidate the discharge behavior at more general Mg GBs, such as twist

[a] Center for Green Research on Energy and Environmental Materials (GREEN) and International Center for Materials Nanoarchitectonics (MANA), National Institute for Materials Science (NIMS), 1-1 Namiki, Tsukuba, Ibaraki 305-0044, Japan.
[b] Elements Strategy Initiative for Catalysts & Batteries (ESICB), Kyoto University, 1-30 Goryo-Ohara, Nishikyo-ku, Kyoto 615-8245, Japan.
[c] PRESTO, Japan Science and Technology Agency (JST), 4-1-8 Honcho, Kawaguchi, Saitama 333-0012, Japan.
[d] Department of Chemical Science and Engineering, Kobe University, 1-1 Rokkodai-cho, Nadaku, Kobe 651-8501, Japan.
[e] Research Center for Structural Materials, National Institute for Materials Science, 1-2-1 Sengen, Tsukuba 305-0047, Japan.
Electronic Supplementary Information (ESI) available: See DOI: 10.1039/x0xx00000x

and tilt GB, the atomic and direct GB models are crucial to extract the reliable mechanism.

In this work, we addressed to elucidate the microscopic correlations among (1) the representative twist and tilt GBs, (2) the alloying elements, and (3) the dissolution/deposition behavior in Mg and Mg-alloys for higher performance of NE, leading to the realization of MRB. We present atomic models for Mg's bulk, surface, and both tilt and twist GB structures with first-principles-based Density Functional Theory (DFT) calculations. In addition to the (0001) surface that has been identified as the most stable surface,[30,31] we also picked the (10$\bar{1}$0) and (11$\bar{2}$0) surfaces, [0001](10$\bar{1}$0) tilt GB, and the [0001](0001) twist GB with different rotating angle (Σ7, Σ13, and Σ19) for a comprehensive investigation. Five alloying elements, Li, Na, Al, Ca, and Zn, were investigated to reveal the alloying effect. Lastly, we proposed a new mechanism of how the GBs tune the conventional electrochemical diagram.

Simulation Method

Atomic bulk, grain boundary, and surface structure

The lattice parameters and atom positions were chosen based on the stable crystal structure of bulk Mg,[32,33] which is hexagonal close-packed (hcp) with a space group of $P6_3/mmc$ in Hermann-Mauguin notation.[34] Generally, the formation energy of the coincident site lattice (CSL) GB is lower than non-CSL GB, and its structure is more stable and mechanically robust.[35,36] Therefore, we chose the CSL GBs in this study. Several misorientation angles can yield CSL GBs, and each corresponds to a sigma (Σ) value that is defined as the reciprocal of the ratio of coincidence sites to the total number of sites. We picked the low Σ values because they contain higher density and are expected to have lower energy,[37,38] which are 21.7868° ($\Sigma 7$), 32.2042° ($\Sigma 13$), and 13.1736° ($\Sigma 19$) in this work (also shown in Supplementary Table 1.

GBs can be categorized into twist and tilt boundaries based on the rotation axis and the GB plane. For the twist GBs, the rotation axis is perpendicular to the GB plane, denoting as $\Sigma 7$ [0001](0001) twist GB. Regarding the tilt GBs, the rotation axis and the GB plane are the same. We picked the (10$\bar{1}$0) GB plane because it yields symmetrical GBs, denoting as $\Sigma 7$[0001](10$\bar{1}$0). Because the rotating axis and the GB plane were not changed in this work, we used $\Sigma 7$ twist or $\Sigma 13$ tilt for GB representations for convenience. Structures of different GB were built via the pymatgen.analysis.gb.grain module in Pymatgen,[39] an open-source Python library for materials analysis. Five GBs, including different numbers of Mg atoms, were selected to be investigated, which are Σ7 twist: Mg336, Σ13 twist: Mg156, Σ19 twist: Mg228, Σ7 tilt: Mg322, and Σ13 tilt: Mg596. Σ19 tilt GB was not considered here because the total Mg atoms will be over 1,000, exceeding our DFT computation capacity. Supercells were used to ensure the lattice parameters are all larger than 10 Å and avoid the interaction between the vacancies or dopants in periodic cells. The length of the c-axis was set at longer than 30 Å to have enough separation between the bulk region and GB region. There is an extra distance between the two grains based on the total energy comparison in Supplementary Table 2. All the atomic GB structures are shown in Supplementary Figure 1. In addition to GB structures, three different Mg surface structures were selected for comparison, (0001), (10$\bar{1}$0), and (11$\bar{2}$0). Supercells were also used to ensure all the lattice parameters are longer than 10 Å, and the vacuum thickness was set at 15 Å to avoid the interaction between slabs. The numbers of the Mg atom are 128, 136, and 176 in (0001), (10$\bar{1}$0), and (11$\bar{2}$0) slab structures, respectively.

The GB energy, which is also called the excess energy of GB,[38] γ, is used to search for the energetic-favorable GB structures and is determined from the energy difference between the GB and the bulk structure via the following equation:[40]

$$\gamma_{Mg} = \frac{E_{GB}^{Mg} - N\mu_{Mg}}{2A} = \frac{E_{GB}^{Mg} - N\frac{E_{bulk}^{Mg}}{n}}{2A} \qquad \text{Eq.1,}$$

where E_{GB}^{Mg} is the total energy of Mg GB (unit: eV), μ_{Mg} is the chemical potential per atom in the Mg hcp bulk structure (unit: eV/atom), which is 1.5051 eV based on our calculation for the bulk Mg supercell with 64 atoms. N and n are the numbers of Mg atoms in the GB and bulk structure, respectively. E_{bulk}^{Mg} is the total energy of the Mg bulk. A is the cross-section area on the *ab* plane in the GB structure (unit: m^2).

For Mg-Alloy, the concentration of the alloying elements is usually high. In this work, we simulated the alloying effect by doping as an approximation. Thus, we use "doping" instead of "alloying" in the results and discussion to avoid confusion. One Mg atom is replaced with one doping atom (Li, Na, Al, Ca, or Zn). Therefore, Eq.1 can be revised to Eq. 2 for calculating the GB excess energy of Mg-alloy GB:

$$\gamma_{Mg+X} = \frac{E_{GB}^{Mg+X} - nE_{bulk}^{Mg+X} - (i\mu_{Mg} + k\mu_X)}{2A} \qquad \text{Eq.2,}$$

where E_{GB}^{Mg+X} and E_{bulk}^{Mg+X} are the total energy of Mg-alloy GB and Mg-alloy bulk, respectively (unit: eV). n is an integer number of the stoichiometric formula units in the GB based on the number of Mg atoms in bulk. i and k are the excess number of Mg atoms and doping atoms, respectively, (positive if it is excess in the GB structure). μ_X is the chemical potential per doping atom in its bulk structure (unit: eV/atom). In this case (Mg-alloy bulk and Σ7 tilt-4V Mg-alloy GB), n, i, and k are 5, 2, and -4 in Eq. 2.

To calculate the E_V, we removed the Mg or doping atom one at a time (the region in between the dashed lines in Supplementary Figure 1). E_V can be calculated as:

$$E_V = E_{defective} + \mu_{Mg}(or\ \mu_X) - E_{initial} \qquad \text{Eq.3,}$$

where $E_{defective}$ and $E_{initial}$ are the total energies of the structure after and before a new vacancy is introduced, respectively.

The dopant segregation energy is used to evaluate the tendency of the dopant moving to GB rather than staying in bulk and can be calculated as:[27,28]

$$E_{segregation} = \left(E_{bulk}^{Mg} - E_{bulk}^{Mg+X}\right) - \left(E_{GB}^{Mg} - E_{GB}^{Mg+X}\right) \qquad \text{Eq.4.}$$

DFT calculation setting

The plane-wave-based DFT calculations were performed via the Vienna Ab initio Simulation Package (VASP).[41] Generalized Gradient Approximation (GGA) of Perdew, Burke, and Emzerhof (PBE)[42] was applied, and the core-valence electron interaction was treated using the projector augmented wave.[43] Valence electron orbitals were selected based on the element: $2s^2 2p^6$ for Mg, $1s^2 2s^1$ for Li, $2p^6 3s^1$ for Na, $3s^2 3p^1$ for Al, $3s^2 3p^6 4s^2$ for Ca, and $4s^2 4d^{10}$ for Zn. Both the lattice and atom positions were relaxed first during the geometry optimization to ensure no internal stress. In further calculations, such as the doping and vacancy effects, only the atom position was relaxed. The convergence criteria of electronic and ionic steps were set at an energy difference of 10^{-5} eV and a force smaller than 0.03 eV/Å, respectively. Cutoff energy of 520 eV and a k-spacing of 0.03 $Å^{-1}$ in the reciprocal space of the Monkhorst–Pack scheme[44] were applied to ensure the convergence of total energy at less than one meV/atom during the geometry optimization. For the DOS calculation, a k-spacing of 0.01 $Å^{-1}$ was used to obtain accurate results. The smearing method of Methfessel-Paxton (order 2) was selected to describe the partial occupancies of orbitals with a width of 0.2 eV, which is suggested for metal calculations.

Results and discussion

Search for energetic-favorable GB structures

The atomic structures of the twist and tilt GB structures with different rotating angles are shown in Supplementary Figure 1, and the corresponding information is listed in Table 1. Figure 1 (a) shows the relative position of different GBs and surfaces selected in this work. The calculated GB excess energies in Table 1 are in good agreement with the other computational studies. It shows the Σ7 is the most energetic-favorable angle for both twist and tilt GBs because of the lowest GB excess energy. To simulate the anodic dissolution of Mg NE, we calculated the vacancy formation energy (E_V) of the Mg atom at the GBs and grain interior (bulk) because the physical meaning of E_V is taking the Mg^{2+} and $2e^-$ all together from the system.[45] E_V can also be used to evaluate the voltage.[46]

Upon calculating the E_V of Mg atoms at the Σ7 tilt GB, we found that some Mg atoms have a negative E_V, as shown in Figure 1 (b). This result implies that these Mg atoms are unstable at the Σ7 tilt GB and will be removed "spontaneously." So, we eliminated the Mg atom with the lowest E_V, relaxed the structure again, and calculated the E_V for the remaining Mg atoms. Repeat the process until all the Mg atoms have a positive E_V that indicates the GB structure reaches stable states. Figure 1 (b) shows that the E_V of Mg atoms became all positive until four Mg atoms were removed, denoting as Σ7 tilt-4V GB. This intrinsically defective GB has a lower GB excess energy, as shown in Table 1. The detailed defective GB structures and the removed Mg positions can be found in Supplemental Figure 2. Therefore, we chose the Σ7 tilt-4V GB structure for further calculations and analysis.

Table 1. Comparison of different GB structures and the corresponding GB excess energy.

	Rotating Angle (^{0})	Cross-section area ($Å^2$)	Number of atoms	GB excess energy, γ_{Mg} (J/m^2)	
				This work	Literature value
Σ7 twist	21.7868	285.89	336	**0.14**	0.14[38] 0.2[47]
Σ13 twist	32.2042	132.84	156	0.15	0.12[38]
Σ19 twist	13.1736	193.01	228	0.15	0.14[38]
Σ7 tilt	21.7868	230.73	322	0.35	0.3[38]
Σ7 tilt-4V	32.2042	230.73	318	**0.32**	
Σ13 tilt	13.1736	431.89	596	0.38	0.35[38]

Vacancy formation energy of Mg atoms in bulk, surfaces, and GBs

To evaluate where the Mg atoms will be stripped from preferentially during discharge, we calculated the E_V of Mg atoms in the bulk, surfaces, and GBs, respectively. The atomic structures are shown in Figure 1 (a). The (0001) surface represents the surface exposed to the electrolyte as it is the most stable surface orientation,[48] so $(10\bar{1}0)$ and $(11\bar{2}0)$ are the sidewalls of Mg NE. The calculated E_V values are shown in Figure 1 (c), compared with the other two GB structures, Σ7 twist GB

and Σ7 tilt-4V GB. The E_V in the bulk Mg hcp structure is ~0.8 eV, while in the Σ7 twist GB and Σ7 tilt-4V GB, most of the Mg atoms near the GB region having an E_V smaller than the bulk value, around 0.2 and 0.35 eV, respectively. Because the physical meaning of E_V refers to taking the Mg-ion and electrons from the system, it represents the energy needed to remove the Mg atom during the discharging process, like an activation barrier. The results indicate that the Mg atoms at the GBs will be stripped preferentially during discharge. Even though the Mg atoms at the twist GBs also have a lower E_V, they may not be involved during the discharge since the [0001](0001) twist GBs locate underneath the (0001) surface, not directly exposed to the electrolyte. Therefore, we focused on the dissolution from the [0001](10$\bar{1}$0) tilt GB for further analysis.

Figure 1 (c) compares the E_V values for different sidewall surfaces as well. It appears that there are two classes of E_V. One is very similar to the bulk value (0.8 eV), while another has a lower value (varying from 0.2 to 0.6 eV). The difference comes from the different positions and coordination environments of Mg atoms. It also explains the broad E_V distribution in GB structures because the atoms near the GB region have various coordination environments. For those Mg atoms at the first surface layer, lower E_V values were observed since they are under-coordinated. The environment of Mg atoms underneath the first surface layers is just like in bulk, resulting in a similar E_V value to that in bulk.

An interesting result lies in the lowest E_V on different surfaces. The (0001) surface has the highest E_V of 0.55 eV, followed by the 0.39 eV on the (10$\bar{1}$0) surface and 0.22 eV on the (11$\bar{2}$0) surface. It indicates that the Mg atoms on the (10$\bar{1}$0) and (11$\bar{2}$0) surfaces are easier taken out than that on the (0001) surface during discharge. This result is also in line with an experimental study investigating the corrosion rate on different surfaces, in which the same trend was observed.[49] Another finding worth mentioning is that there are some positions at the tilt GB and on the side surfaces with a higher E_V (around 0.9 eV) than in bulk (0.8 eV). Contrary to the low E_V positions that favor the dissolution process, the high E_V positions are the favorable sites during deposition. While on the (0001) surface and twist GB, such high E_V positions do not exist. Therefore, the tilt GB and the side surfaces not only accelerate the dissolution (discharge) but also help the deposition (charge). A more detailed mechanism regarding the electrode reactions with GBs is discussed in the Discussion part.

By combining GB and surface results, we suppose that the Mg atoms will be oxidized and removed preferentially from the tilt GBs and sidewalls on the (0001) surface during discharge because of the lower E_V, resulting in a pit-type dissolution that was also observed in the experiments.[50] The agreement with experiments validated our method that correlates the E_V with the morphology change at different surfaces and GBs. Also, note that the lowest E_V of 0.38 eV on the Σ7 tilt-4V GB is very close to the value on the (10$\bar{1}$0) surface. It is because the rotating plane of the tilt GB in this work was selected to be (10$\bar{1}$0) plane. Therefore, at the position with the longest distance between two grains, the coordination environment is similar to the (10$\bar{1}$0) surface.

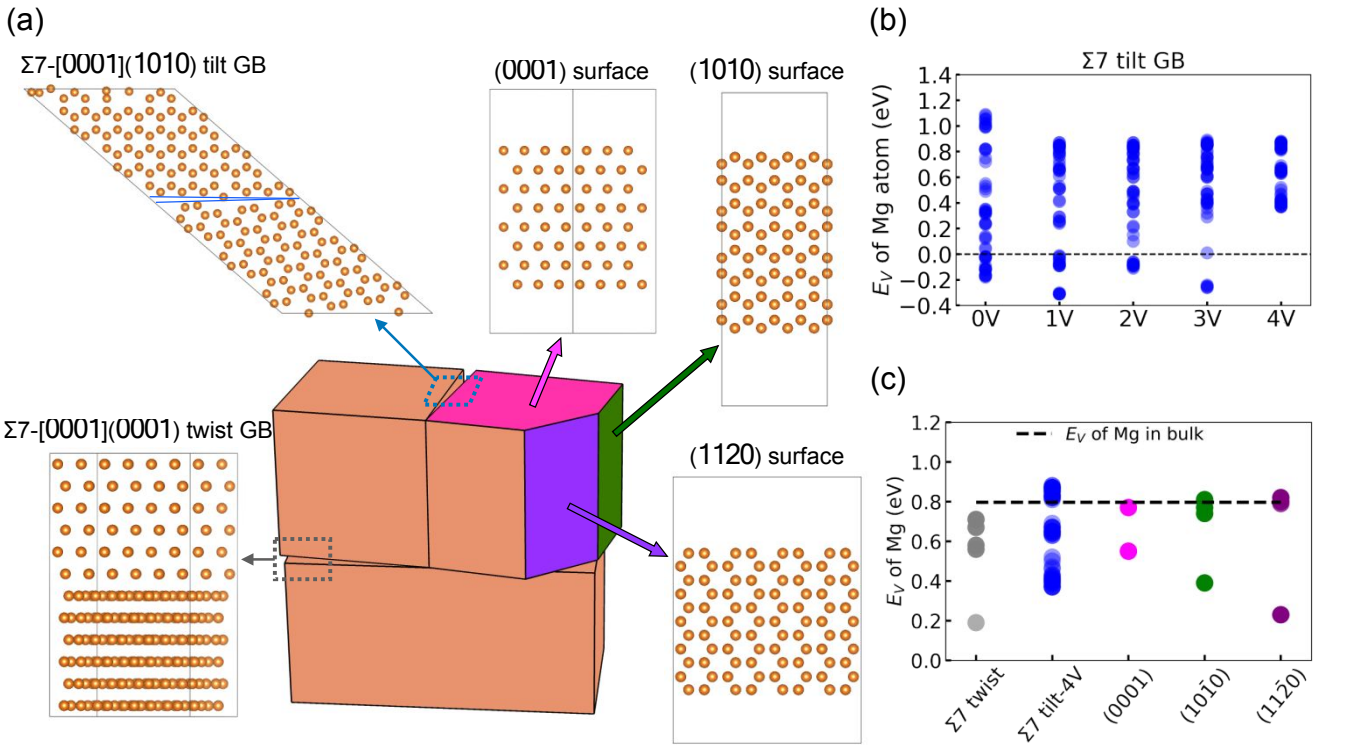

Figure 1. (a) Atomic structures and the orientations of the surfaces and GBs investigated in this work. The tilt and twist GB structures with different rotating angles (Σ7, Σ13, and Σ19) can be found in Supplementary Figure 1. (b) The Mg atoms near the GB plane in Σ7 tilt GB were removed one at a time (1V means 1 Mg atom was removed) until all the Mg atoms

in the structure have a positive E_V (Σ7 tilt-4V). (c) Comparison of E_V of Mg atoms between Mg bulk, surfaces, and GBs. For the GBs, only the structures with the lowest GB excess energy (Σ7 twist and Σ7 tilt-4V), as shown in Table 1.

The impact of the local environment on E_V at the GBs

To reveal the cause of the broad distribution of E_V at GBs, we compared the local environment (atom distance between neighboring atoms) of Mg atoms at the GB region, and the results are shown in Figure 2. For the Σ7 twist GB, the atomic distances are 2.60 – 2.86 Å with E_V of 0.19 – 0.56 eV, smaller than the bond length of 3.18 Å in the Mg bulk. The shorter distance between the Mg atoms at the twist GB increases the total energy. Thus, removing the Mg atoms from the twist GB is more favorable than from the bulk because it avoids the short distance between Mg atoms and relaxes the local environment.

Unlike the Σ7 twist GB, at the Σ7 tilt-4V GB, some of the bond lengths are shorter than that bulk bond length (3.18 Å), while others are longer, as shown in Figure 2 (b). The same trend also reflects on the E_V value. Mg atoms with a shorter bond length have an E_V value of 0.40 – 0.65 eV, smaller than the bulk E_V value of 0.79 eV. For the Mg atoms with a longer distance with neighboring atoms (at least 3.4 Å), the E_V value is around 0.88 eV, higher than the bulk value. Therefore, the broad distribution of E_V at GBs in Figure 1 (c) can be attributed to the local environment and the bond length variation.

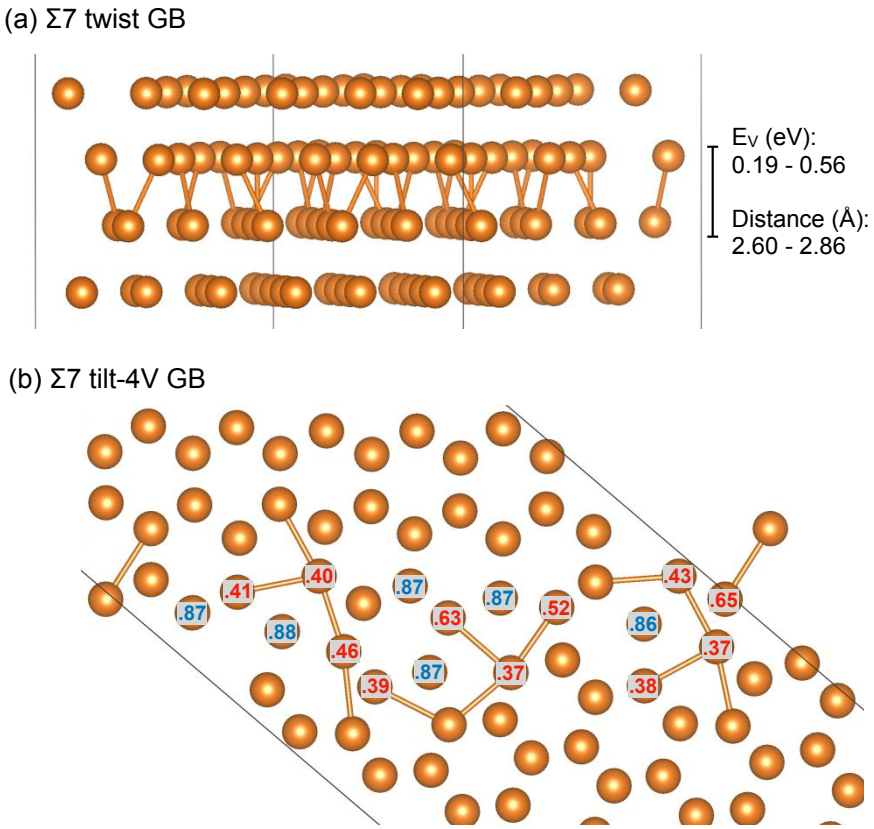

Figure 2. Relaxed atomic structures near the (a) Σ7 twist GB and (b) Σ7 tilt-4V GB with corresponding E_V values of each Mg atoms. The cutoff bond length in this plot is 3.05 Å, and the bond length in the Mg bulk is 3.18 Å. The numbers labeled with blue and red in (b) represent the E_V larger and smaller than the bulk value (0.79 eV), respectively. The values labeled in (b) are simplified by removing the leading zero. For example, .88 refers to 0.88 eV.

The effect of doping on the GB excess energy

To investigate the doping effect in the Mg electrodes, we replaced a single Mg atom at different positions with a single doping atom (Na, Ca, Al, Zn, or Li) within the GB region (between the dashed lines in Supplementary Figure 1 and the structure with the lowest energy was used as the representative Mg-alloy GB structures. We considered only the Σ7 tilt-4V GB in this part because the tilt GB is the one that contributes to the pit-type morphology observed on the surface of Mg NE during the discharge. Firstly, the effect of different doping elements on the GB excess energy was calculated via Eq. 2 and compared in Table 2. It can be seen that the GB excess energy changes from the original 0.32 J/m^2 to 0.25 J/m^2 (Na) and 0.34 J/m^2 (Li) after doping. Note that the physical meaning of Eq.2 is the excess energy of the Mg-alloy GB over the Mg-alloy bulk. A lower GB excess energy means that it is easier to create such GB. Therefore, it is expected that if doping with Na or Ca, more tilt GBs will be formed in Mg NE. On the other hand, if doping with Li, it may reduce the amount of tilt GBs. This result may relate

to a previous experimental work, in which the addition of Ca was found to create more GBs and result in more cracks during discharge.[13]

Table 2. Comparison of the total energy and the GB excess energy before and after doping with different elements in Σ7 tilt-4V GB.

Doping element	Energy of Mg-alloy bulk, E_{bulk}^{Mg+X}, 64 atoms (eV)	Energy of Mg-alloy GB, E_{GB}^{Mg+X}, 318 atoms (eV)	Chemical potential of doping atom, μ_X (eV/atom)	GB excess energy (J/m^2)
Pure Mg	-96.33	-469.49	-1.51(μ_{Mg})	0.32
Na	-95.77	-469.33	-1.34	**0.25**
Ca	-96.78	-470.73	-2.00	**0.28**
Al	-98.57	-471.86	-3.75	**0.31**
Zn	-96.17	-469.64	-1.27	0.32
Li	-96.89	-470.14	-1.91	0.34

The reason why doping elements behave differently at the tilt GB

The tendency of doping atoms staying in the grain interior or moving to the GB can be determined by the GB segregation energy (Eq. 4), and the results are shown in Figure 3 (a). A negative GB segregation energy means the doping element prefers to move to the GB rather than in the grain interior. We took the lowest GB segregation energy to compare the different doping elements since it is the most stable structure. It can be seen that Ca has the most negative GB segregation energy, around -0.8 eV, followed by -0.4 eV of Na. Li has the highest GB segregation energy of around -0.1 eV. It indicates that all the tested doping elements tend to move to the GB region, and Ca has the strongest driving force to move. The results agree with another experimental study, where the Al concentration at the GBs in the Mg-alloy is increased.[51]

To further investigate why different doping elements at the tilt GB have such different distributions in GB segregation energy, we compared the local environment of the most energetic-favorable site for each doping atom, as shown in Figure 3 (b). At the tilt GB, due to the triangle-like contact between the grains, space could be larger or smaller than that in the Mg bulk, as the Mg-A and Mg-B in Figure 3 (b). Interestingly, Ca and Na both prefer to replace the Mg-A atom, and Li, Al, and Zn all prefer to replace the Mg-B atom. While checking the atom distances with the neighboring Mg atoms, it appears that the Mg-A environment is relatively large, with all distances longer than 3.3 Å. On the other side, the Mg-B environment has shorter atom distances than 3.13 Å with the neighboring Mg atoms. If taking the atomic distance of 3.18 Å in Mg bulk as a reference, Mg-A is like in a large "cave." The different favorable positions could be attributed to the atomic radius of the doping elements, as shown in Figure 3 (b). Ca and Na with a radius of around 190 pm are relatively larger than all the other doping elements and Mg atom (145 pm). Therefore, they fit the large cave at the tilt GB, which results in a more negative GB segregation energy. For the smaller doping atoms, Li, Al, and Zn, the small cave is more favorable. However, at the tilt GB, the small cave may not be small enough for these smaller doping elements to stabilize it, so the GB segregation energy is not that negative compared with the larger doping elements. A particular case is the Li doping, in which the Li atom radius (167 pm) is larger than the Mg atom, but its energetic-favorable replacing position is the small cave (Mg-B). It means the large cave (Mg-A) is too large for it, but the small cave will be too crowded. As a result, Li doping in the tilt GB introduces a relatively larger GB segregation energy (-0.1 eV), close to zero, indicating less tendency to move the tilt GB than other doping elements.

Combining with the GB excess energy results after doping in Table 2, we can expect that doping with Na and Ca in Mg, more tilt GBs (sidewall at the Mg surface) will be formed, and these doping elements will migrate to the GBs. According to the results that the E_V of Mg atoms is much smaller at the GBs than in bulk, doping with Ca or Na accelerate the dissolution rate of Mg NE, and so the discharging rate and current density increase. According to previous studies,[52,53] Li, Al, Ca, and Zn, have been experimentally found to sufficiently dissolve into Mg, such as AZ91 (9 wt% Al and 1 wt% Zn in Mg) and LZ91 (9 wt% Li and 1 wt% Zn in Mg). These alloying elements (Li, Al, and Zn) are capable of reducing the passivation layers but may not be as suitable as Ca in terms of more tilt GBs. Thus, Ca is the best candidate to increase Mg NE performance among the tested doping elements in this work.

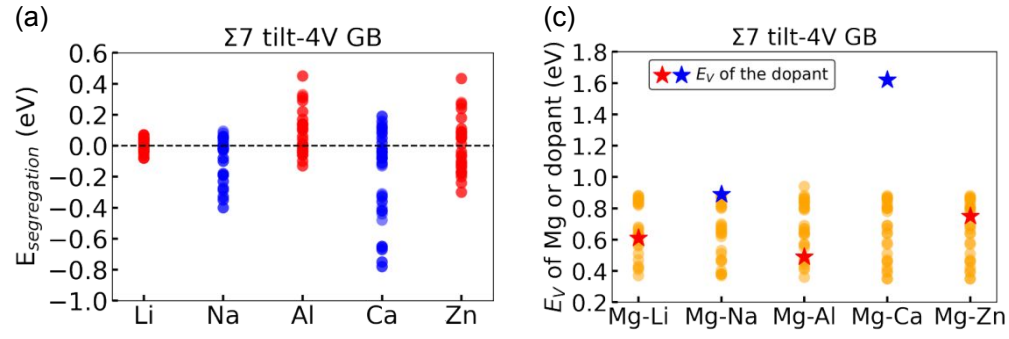

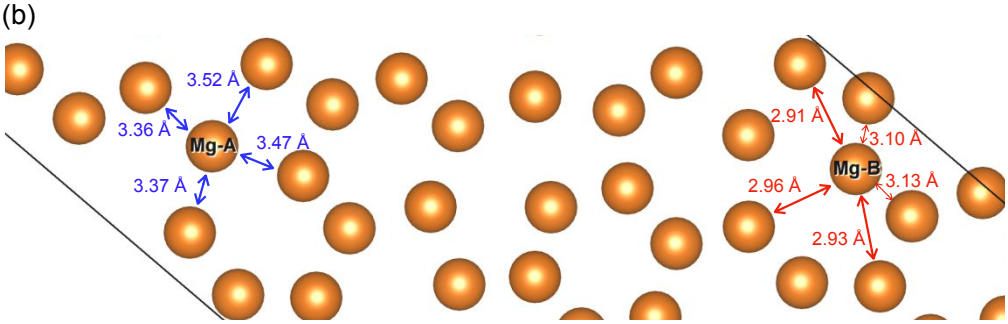

Atomic radius (pm)					
Mg	Li	Na	Al	Ca	Zn
145	167	190	118	194	142

Figure 3. (a) Comparison of the GB segregation energy at the Σ7 tilt-4V GB with different dopants. Each data point corresponds to one of the replaced Mg atoms in the GB region. (b) Relaxed structure of Σ7 tilt-4V GB. Mg-A is the most energetic-favorable position for Na and Ca, while Mg-B is for Li, Al, and Zn. Atom distances with blue color are longer than that in bulk (3.18 Å), while red colors represent the shorter atom distance. The value of the atomic radius for each element was taken from the reference.[54] (c) Comparison of E_V of Mg atoms (circles) and doping atoms (stars) in Σ7 tilt-4V GB.

The effect of doping on the E_V of Mg atoms at GBs and surfaces

Doping with different elements at the GB may change the E_V of surrounding Mg atoms and affect the intrinsic dissolution performance. Figure 3 (c) shows the calculated E_V of Mg atoms at the tilt GB after doping. The distributions of E_V value of Mg atoms are almost identical to the results of pure Mg (Figure 1 (c)), ranging from 0.3 to 0.9 eV. The results imply that doping will not change the dissolution performance of Mg atoms from the tilt GB. An interesting result is the E_V of the doping atom. Most of them, Li, Na, Al, and Zn, have an E_V value within Mg's values (0.3 to 0.9 eV), indicating a similar dissolution tendency during discharge.

Regarding the Ca doping, however, its E_V at the tilt GB is around 1.6 eV that is much higher than all the Mg atoms and the other doping elements. It implies that the Ca atom at the tilt GB is relatively stable and probably will not be removed during discharge. The exceptional stability of Ca at the Mg tilt GB can be attributed to the size effect discussed above. The Ca atom fits the large cave in the Mg tilt GB stably. Note that the Ca metal has a relatively negative standard electrode potential, -2.76 V vs. standard hydrogen electrode (SHE), compared with Mg metal of -2.37 V vs. SHE. Theoretically, Ca metal has a higher tendency to be oxidized than Mg metal. However, in the situation of Ca alloying in Mg, the electronic property of the Ca atoms in the Mg metal could be completely different from in the Ca metal, which may result in a more positive standard potential for Ca atoms in the Mg metal.

The electronic properties of the bulk structures and the tilt GB structures before and after doping were also compared. Supplementary Figure 3 shows the projected density of states (PDOS). For the bulk and GB of pure Mg, it appears that the intensity of PDOS of the tilt GB structure near the Fermi level is slightly higher than the bulk structure, implying a higher current density at the tilt GB. Nevertheless, there is no apparent change in Mg PDOS after doping with different elements.

We have also examined the Ca doping effect at the Mg-Ca surface, as shown in Supplementary Figure 4 and Supplementary Figure 5. The E_V distributions of Mg at the Mg-Ca surfaces are similar to that at the pure Mg surfaces, ranging from 0.2 eV to 0.8 eV, meaning that the Ca doping does not change the Mg stripping tendency at the surfaces as well. An interesting result lies on the E_V of Ca at the Mg-Ca surface, which is around 0.55 eV – 0.75 eV, not much different from and even lower than some Mg atoms. The results are pretty different from the 1.6 eV of Ca E_V at the Mg-Ca tilt GB in Figure 3 (c). It indicates that the Ca at the Mg-Ca surfaces is possible to be removed after some Mg atoms with lower E_V are stripped. Although based on Figure 3 (a), Ca atoms tend to move to GBs, it is still evitable that a small amount of Ca will be staying at the surfaces if considering the kinetics and temperature effects. Therefore, it is expected that some Ca will be removed and dissolved in the electrolyte after cycling. A recent publication has also observed such phenomena. [55]

Based on this result, the effect of doping in Mg NE has less impact on the intrinsic dissolution tendency of Mg atoms. Instead, doping plays a more critical role in enhancing more GBs, and then the dissolution performance.

Proposed mechanism of the GB effects on the Mg electrode kinetics

How the microstructures, such as GBs and defects, affect the electrode kinetics is crucial to optimize the Mg NE performance. However, a detailed discussion of the underlying mechanism remains unclear, and the number of relevant studies is limited. In this work, we propose a mechanism by connecting the results of our calculations to the conventional free energy diagram between Mg^{2+} + $2e^-$ and Mg, as shown in Figure 4 (a). The calculated E_V of Mg atoms (Figure 1 (c)) can be correlated to the reaction barrier. A lower E_V (0.3 eV) implies the barrier of the anodic reaction (Mg^{2+} + $2e^-$ → Mg) decreases, while a higher E_V (0.9 eV) indicates a lowered barrier for cathodic reaction. Note that the 0.9 eV is in the condition that the GB is fully occupied (charged state). Upon discharge, some of the Mg atoms will be removed, and the GB atomic structure will be reconstructed, which may create more space for Mg atoms to be deposited during charge. It is expected that those sites with larger space will have a larger E_V than 0.9 eV, as the effect of the local environment that we discussed in Figure 2 (b). Therefore, the existence of tilt GBs and the $(10\bar{1}0)$ and $(11\bar{2}0)$ surfaces (sidewalls with respect to the (0001) surface, as Figure 1 (a) shows) effectively decreases the barrier of anodic and cathodic reactions. The connection between the E_V of Mg and the activation energy is also proposed by recent theoretical papers,[56,57] while the site effect and the local environment of Mg atoms, especially at the GBs, have not been discussed yet.

.

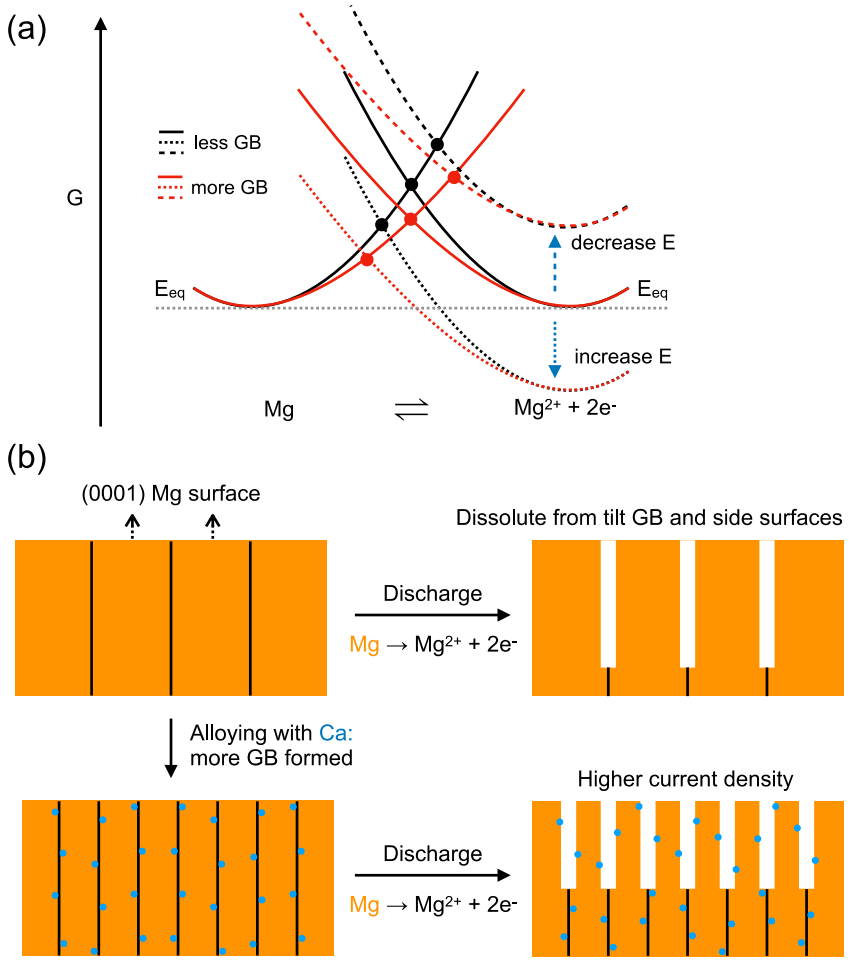

Figure 4. (a) Conventional free energy (G) diagram of reactions between Mg and Mg^{2+} + $2e^-$. Black and red lines represent the Mg electrode with lower and higher GB density, respectively. E refers to the electrode potential, and E_{eq} is the equilibrium potential. Black and red dots are used to emphasize the points with the highest G along the reaction coordinate. (b) Schematic of the effect of tilt GBs and side surfaces, and the alloying on the performance of the Mg electrode.

A recent experimental paper[55] showed that the Mg electrodes with more refined grains (more GBs) or doping with Ca resulted in a higher current density during charge and discharge, and the current density maintained almost symmetrical in all the cases. It implies that the value of the charge transfer coefficient (usually denoted as α) in the

electrode kinetics expressed by the Bulter-Volmer equation is close to 0.5. Thus, we speculate that the reduction of reaction barriers by tilt GBs is likely symmetrical for both anodic and cathodic reactions, illustrated as the identical slope change in Figure 4 (a) (from the black line to the red line). Because the charge transfer coefficient is kept at 0.5, the reaction barrier reduction contributes to a larger exchange current density (usually denoted as I_0) in the Bulter-Volmer equation. As a result, no matter the applied potential (E) is more positive or negative than the equilibrium potential (E_{eq}), the current density will be increased if there are more tilt GBs. The adsorption of inactive species, as reported before[58], and the passivation formation will affect the current density as well. We have not included the effect of passivation layers yet, such as MgO or $Mg(OH)_2$, whose amount may increase with the GB density and negatively impact the electrode performance. However, experimental studies[55] did not observe a decrease in current density for the Mg electrode with fewer GBs. Therefore, we suppose the effect of the passivation layers is limited in this case.

Figure 4 (b) illustrates the main concept of the dissolution mechanism proposed in this work. Upon discharge, the Mg atoms will preferentially be stripped from the tilt GBs and the side surfaces, which enhance the discharging current density, resulting in a pit-type morphology. If doping with Ca, more tilt GBs will be formed, and the Ca atoms will aggregate at the GBs. The discharge performance is further enhanced

Conclusions

We investigate the effects of the tilt GBs and different alloying elements on the electrochemical performance of the Mg and Mg-alloy NE via a first-principles DFT model. Based on our calculations of E_V, the Mg atoms at the $[0001](10\bar{1}0)$ tilt GB and the side surfaces, $(10\bar{1}0)$ and $(11\bar{2}0)$, relative to the stable (0001) surface, are much easier to be stripped during discharge and so the current density enhanced. The broad distribution E_V of Mg atoms at the tilt GB can be attributed to the local environment. Alloying Mg with other elements, including Li, Na, Al, Ca, and Zn that were investigated in this work, will not change the intrinsic dissolution tendency of Mg atoms at the tilt GB. Instead, alloying with certain elements, such as Na and Ca, can create more tilt GB than Li, Al, or Zn, resulting in improved discharge performance. According to the GB segregation energy results, all the alloying elements prefer to move to the tilt GB rather than staying in bulk. The different behaviors between alloying elements are also determined by the local environment at the tilt GB, where Ca is relatively stable than all the others.

We have also proposed a new mechanism of how the GB affects the Mg electrode kinetics by correlating our DFT results with the conventional diagram of standard free energy. We speculated that the existence of tilt GB at the Mg surface essentially decreases the reaction barriers for both the anodic and cathodic reactions symmetrically and enhances the exchange current density. Therefore, a higher tilt GB density is beneficial to the discharge/charge performance of Mg NE, which can be tuned by different alloying elements. Nevertheless, more GBs usually cause a decrease in the mechanical strength of the electrode. A future work considering the balance between the tilt GB density and the mechanical strength may be necessary.

Conflicts of interest

There are no conflicts to declare

Acknowledgements

This work was supported in part by JST ALCA-SPRING Grant Number JPMJAL1301, by JSPS KAKENHI Grant Number JP19H05815, and by MEXT as “Program for Promoting Researches on the Supercomputer Fugaku (Fugaku Battery & Fuel Cell Project), Grant Number JPMXP1020200301. The calculations were carried out on the supercomputers at NIMS and The University of Tokyo. This research also used computational resources of the supercomputers at the RIKEN and the HPCI Systems through the HPCI System Research Project (project ID: hp200131 and hp210173). We appreciate the developer of a Fortran 90 program, VASPKIT, which helped the pre- and post-process of the VASP data and structures. (V. Wang, N. Xu, VASPKIT: A Pre- and Post-Processing Program for the VASP Code. http://vaspkit.sourceforge.net.)

References

1 D. Aurbach, Z. Lu, A. Schechter, Y. Gofer, H. Gizbar, R. Turgeman, Y. Cohen, M. Moshkovich and E. Levi, *Nature*, 2000, **407**, 724–727.

2 D. Linden, in *Choice Reviews Online*, 1995, vol. 33, pp. 33-2144-33–2144.

3 H. D. Yoo, I. Shterenberg, Y. Gofer, G. Gershinsky, N. Pour and D. Aurbach, *Energy Environ. Sci.*, 2013, **6**, 2265–2279.

4 M. Matsui, *J. Power Sources*, 2011, **196**, 7048–7055.

5 T. Zhang, Z. Tao and J. Chen, *Mater. Horizons*, 2014, **1**, 196–206.

6 D. Cao, L. Wu, G. Wang and Y. Lv, *J. Power Sources*, 2008, **183**, 799–804.

7 A. Pardo, M. C. Merino, A. E. Coy, F. Viejo, R. Arrabal and S. Feliú, *Electrochim. Acta*, 2008, **53**, 7890–7902.

8 N. Wang, R. Wang, C. Peng, B. Peng, Y. Feng and C. Hu, *Electrochim. Acta*, 2014, **149**, 193–205.

9 N. Singh, T. S. Arthur, C. Ling, M. Matsui and F. Mizuno, *Chem. Commun.*, 2013, **49**, 149–151.

10 B. Huang, Z. Pan, X. Su and L. An, *J. Power Sources*, 2018, **395**, 41–59.

11 A. A. Nayeb-Hashemi, J. B. Clark and A. D. Pelton, *Bull. Alloy phase diagrams*, 1984, **5**, 365–374.

12 Y. Song, D. Shan, R. Chen and E. H. Han, *Corros. Sci.*, 2009, **51**, 1087–1094.

13 M. Yuasa, X. Huang, K. Suzuki, M. Mabuchi and Y. Chino, *J. Power Sources*, 2015, **297**, 449–456.

14 M. Deng, D. Höche, S. V. Lamaka, D. Snihirova and M. L. Zheludkevich, *J. Power Sources*, 2018, **396**, 109–118.

15 J. Liu, Y. Song, J. Chen, P. Chen, D. Shan and E. H. Han,

Electrochim. Acta, 2016, **189**, 190–195.
16 H. Xiong, K. Yu, X. Yin, Y. Dai, Y. Yan and H. Zhu, *J. Alloys Compd.*, 2017, **708**, 652–661.
17 K. Hagihara, M. Okubo, M. Yamasaki and T. Nakano, *Corros. Sci.*, 2016, **109**, 68–85.
18 N. Wang, Y. Mu, W. Xiong, J. Zhang, Q. Li and Z. Shi, *Corros. Sci.*, 2018, **144**, 107–126.
19 J. He, Y. Mao, Y. Gao, K. Xiong, B. Jiang and F. Pan, *J. Alloys Compd.*, 2019, **786**, 394–408.
20 T. Zheng, Y. Hu and S. Yang, *J. Magnes. Alloy.*, 2017, **5**, 404–411.
21 Y. Savguira, T. H. North and S. J. Thorpe, *Mater. Corros.*, 2016, **67**, 1068–1074.
22 N. N. Aung and W. Zhou, *Corros. Sci.*, 2010, **52**, 589–594.
23 B. Jiang, Q. Xiang, A. Atrens, J. Song and F. Pan, *Corros. Sci.*, 2017, **126**, 374–380.
24 Y. Shi, C. Peng, Y. Feng, R. Wang and N. Wang, *Mater. Des.*, 2017, **124**, 24–33.
25 T. Zhang, Y. Shao, G. Meng, Z. Cui and F. Wang, *Corros. Sci.*, 2011, **53**, 1960–1968.
26 J. F. Nie, Y. M. Zhu, J. Z. Liu and X. Y. Fang, *Science (80-.).*, 2013, **340**, 957–960.
27 H. Somekawa, A. Singh, R. Sahara and T. Inoue, *Sci. Rep.*, 2018, **8**, 1–9.
28 D. A. Basha, R. Sahara, H. Somekawa, J. M. Rosalie, A. Singh and K. Tsuchiya, *Scr. Mater.*, 2016, **124**, 169–173.
29 H. Ma, M. Liu, W. Chen, C. Wang, X. Q. Chen, J. Dong and W. Ke, *Phys. Rev. Mater.*, 2019, **3**, 53806.
30 C. Ling, D. Banerjee and M. Matsui, *Electrochim. Acta*, 2012, **76**, 270–274.
31 C. G. Johansen, H. Huang and T. M. Lu, *Comput. Mater. Sci.*, 2009, **47**, 121–127.
32 A. W. Hull, *Phys. Rev.*, 1917, **10**, 661–696.
33 G. V Raynor and W. Hume-Rothery, *J. Inst. Met.*, 1939, **65**, 379–387.
34 G. Calestani, *Introduction to crystallography*, Courier Corporation, 2002, vol. 123.
35 Y. Ikuhara, *J. Ceram. Soc. Japan*, 2001, **109**, S110–S120.
36 T. Watanabe, *Res Mech. Int. J. Struct. Mech. Mater. Sci.*, 1984, **11**, 47–84.
37 X. Zhu, G. Zhang and C. Yan, in *Study of Grain Boundary Character*, InTechOpen, 2017, pp. 144–159.
38 X. Liu and J. Wang, *Sci. Rep.*, 2016, **6**, 1–8.
39 S. P. Ong, W. D. Richards, A. Jain, G. Hautier, M. Kocher, S. Cholia, D. Gunter, V. L. Chevrier, K. A. Persson and G. Ceder, *Comput. Mater. Sci.*, 2013, **68**, 314–319.
40 T. Uesugi and K. Higashi, in *Journal of Materials Science*, 2011, vol. 46, pp. 4199–4205.
41 G. Kresse and J. Furthmüller, *Phys. Rev. B - Condens. Matter Mater. Phys.*, 1996, **54**, 11169–11186.
42 J. P. Perdew, K. Burke and M. Ernzerhof, *Phys. Rev. Lett.*, 1996, **77**, 3865–3868.
43 P. E. Blöchl, *Phys. Rev. B*, 1994, **50**, 17953–17979.
44 J. D. Pack and H. J. Monkhorst, *Phys. Rev. B*, 1977, **16**, 1748–1749.
45 C. D. Taylor, M. Neurock and J. R. Scully, *J. Electrochem. Soc.*, 2008, **155**, C407.
46 J. Haruyama, K. Sodeyama, L. Han, K. Takada and Y. Tateyama, *Chem. Mater.*, 2014, **26**, 4248–4255.
47 H. Zheng, X. G. Li, R. Tran, C. Chen, M. Horton, D. Winston, K. A. Persson and S. P. Ong, *Acta Mater.*, 2020, **186**, 40–49.
48 J.-J. Tang, X.-B. Yang, L. OuYang, M. Zhu and Y.-J. Zhao, *J. Phys. D. Appl. Phys.*, 2014, **47**, 115305.
49 G.-L. L. Song, R. Mishra and Z. Xu, *Electrochem. commun.*, 2010, **12**, 1009–1012.
50 N. Wang, Y. Mu, Q. Li and Z. Shi, *RSC Adv.*, 2017, **7**, 53226–53235.
51 R. Liang, Y. Su, X. L. Sui, D. M. Gu, G. S. Huang and Z. B. Wang, *J. Solid State Electrochem.*, 2019, **23**, 53–62.
52 H. Okamoto and T. B. Massalski, *Alloy Phase Diagrams*, 2018, 89–89.
53 H. Somekawa, *Mater. Trans.*, 2020, **61**, 1–13.
54 E. Clementi, D. L. Raimondi and W. P. Reinhardt, *J. Chem. Phys.*, 1967, **47**, 1300–1307.
55 T. Mandai and H. Somekawa, *Chem. Commun.*, 2020, **56**, 12122–12125.
56 H. Ma, X. Q. Chen, R. Li, S. Wang, J. Dong and W. Ke, *Acta Mater.*, 2017, **130**, 137–146.
57 Z. Liu, Y. Li, Z. Liu, Y. Li, Y. Ji, Q. Zhang, X. Xiao and Y. Yao, *Cell Reports Phys. Sci.*, 2021, 100294.
58 O. Tutusaus, R. Mohtadi, N. Singh, T. S. Arthur and F. Mizuno, *ACS Energy Lett.*, 2017, **2**, 224–229.